MULTISCALE OPPONENT APPROACH FOR HYPERSPECTRAL TEXTURE RECOGNITION USING AVIRIS DATA

Miaohong Shi and Glenn Healey*

1 Introduction

Hyperspectral sensors measure spectral radiance for a number of contiguous spatial locations to form an image. Several imaging spectrometers provide spectral coverage with hundreds of bands over the visible through short-wave infrared from 0.40 to 2.45 micrometers (Basedow et al., 1995) (Vane et al., 1993) (Simi et al., 2000). Hyperspectal data with its high spectral resolution may be used to identify specific features on the earth's surface such as soils with different composition.

Developing efficient methods to process hyperspectral data becomes important as the number of spectral bands increases. Many existing algorithms for processing hyperspectral data are the direct outgrowth of algorithms that were developed for single band or multispectral sensors where the number of bands is small. These approaches resort to a variety of approximations to reduce the computational burden. Important questions for these approaches include which data-reduction procedure to use and which features to compute.

A large number of techniques for analyzing image texture have been proposed (Haralick, 1979) (Reed et al., 1993). Recent work on texture analysis mainly focuses on statistical approaches and filter-based approaches. The statistical approach characterizes textures as arising from probability distributions on random fields. This approach typically uses a small number of parameters to provide a concise representation for textures. Markov random fields (MRF) (Cross et al., 1983) (Li, 1995) are a popular statistical model for texture. However, these models require prior selection of spatial structure. Multiband correlation models allow for a more generic representation and have been used for geometry-invariant recognition (Kondepudy et al., 1994) and illumination-invariant recognition (Healey et al., 1996) (Healey et al., 1995). Filter-based approaches (Daugman, 1985) (Mallat, 1989) are inspired by multi-channel filtering mechanisms in human vision. Gabor filters have been used extensively to compute texture features for image interpretation tasks (Bovik et al., 1990) (Jain et al., 1991) (Manjunath et al., 1996). These filters achieve optimal joint localization in space and spatial frequency (Daugman, 1985) and can be used to decompose images into components corresponding to different scales and orientations.

The modeling of hyperspectral textures is important for many applications including terrain classification and material identification. The number of spectral bands in hyperspectral imagery provides a large number of spectral/spatial correlations that can be exploited for texture modeling. There have been few attempts to

*Department of Electrical and Computer Engineering, University of California, Irvine, CA 92697 (mshi@ece.uci.edu;healey@ece.uci.edu)

exploit texture information in hyperspectral images. Schweizer and Moura (Schweizer et al., 2001) used Gaussian Markov random fields to model hyperspectral textures to support detection applications.

In this paper, we introduce a representation for hyperspectral textures using unichrome and opponent features computed from Gabor filter outputs. The unichrome features are computed from the spectral bands independently while the opponent features combine information across different bands at different scales. Using an AVIRIS data set acquired at Indian Pines in 1992, we evaluate the performance of the multiscale approach using opponent features for recognizing hyperspectral textures.

2 The Gabor Texture Features

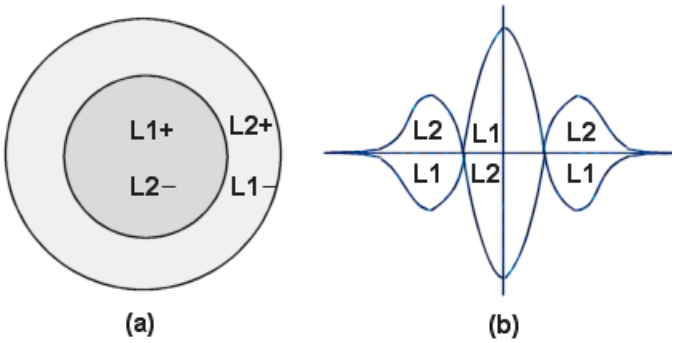

Figure 1: Gabor function approximation of type II opponent cell

Gabor filters are defined in the spatial domain by

$$f_{mn}(x,y) = \frac{1}{2\pi\sigma_m^2}\exp\left(-\frac{x^2+y^2}{2\sigma_m^2}\right) \times \cos(2\pi(u_m x\cos\theta_n + u_m y\sin\theta_n)) \quad (1)$$

where m is the index for the scale and n is the index for the orientation. We consider a filter bank with two scales and four orientations ($0°, 45°, 90°$ and $135°$).

2.1 Unichrome features

Unichrome features are extracted from a single spectral band. Let $L_i(x,y)$ be the ith spectral channel of a hyperspectral image and let $f_{mn}(x,y)$ be a filter in the filterbank. Denote the filtered image

$$h_{imn}(x,y) = L_i(x,y) * f_{mn}(x,y) \quad (2)$$

and the unichrome feature U_{imn} by

$$U_{imn} = \sqrt{\left(\sum_{x,y} h_{imn}^2(x,y)\right)} \quad (3)$$

For C spectral channels, M scales, and N orientations, a set of CMN unichrome features can be computed.

2.2 Opponent features

Hering's opponent process theory (Goldstein, 1996) of human color vision was formulated in the 1800's and later experimentally tested by Hurvich and Jameson (Hurvich et al., 1957). The theory is still a subject of strong interest (Masland, 1996). We can use Gabor functions to model receptive field structure on the retina. For example, we can approximate a type II cell response (Wiesel et al., 1966) using the difference of Gabor functions at the same scale (see Fig. 1). For filtered bands $h_{imn}(x, y)$ and $h_{jmn}(x, y)$, we consider the normalized difference

$$d_{ijmn}(x, y) = \left(\frac{h_{imn}(x, y)}{U_{imn}} - \frac{h_{jmn}(x, y)}{U_{jmn}} \right) \tag{4}$$

Then the type II opponent feature ψ_{ijmn} (Wiesel et al., 1966) (Jain et al., 1998) is obtained by

$$\psi_{ijmn} = \sqrt{\left(\sum_{x,y} d^2_{ijmn}(x, y) \right)} \tag{5}$$

By normalization in (4), we remove information that is already contained in the unichrome features of (3). The opponent features capture the spatial correlation between different spectral channels at a certain scale and orientation.

3 Experiments

3.1 Data set

We used AVIRIS (Vane et al., 1993) hyperspectral data for our experiments from Purdue University's MultiSpec web site[1]. The 20m GSD data was acquired over the Indian Pine Test Site in Northwestern Indiana in 1992. Band 8 (0.58–0.62μm) of this data is shown in Fig. 2. From the data, we obtained 50 test texture images of size 10×10 pixels which belong to the following 8 texture classes: Corn-notill, Corn-min, Soybean-notill, Soybean-min, Grass/Trees, Grass/Pasture, Woods, and Hay-windrowed.

3.2 Band reduction

As the number of spectral channels increases, the ability to discriminate similar ground cover classes should also increase. Often the number of pixels available to texture classification techniques is limited, thus limiting the accuracy with which texture characteristics can be estimated. From the 220 AVIRIS bands, we chose a 126 band subset by excluding bands with low signal due to water absorption or the solar radiance function. Fig. 3 plots an AVIRIS spectral radiance function using the 126-band data set. In order to reduce the dimension of the spectral space, we average every three adjacent spectral bands of the 126 spectral bands to get 42 spectral bands. This significantly reduces feature computation requirements. Fig. 4 shows the spectral radiance function corresponding to figure 3 in the reduced band system using the 42 spectral bands.

3.3 Feature subset selection

For filters defined using 2 scales and 4 orientations, there are a total of 336 unichrome features for the 42 spectral bands. We compute opponent features ψ_{ijmn} for all i, j with $i = 1, 2, \ldots, 42$; $j = 1, 2, \ldots, 42$ and $i \neq j$

[1] http://dynamo.ecn.purdue.edu/~biehl/MultiSpec/

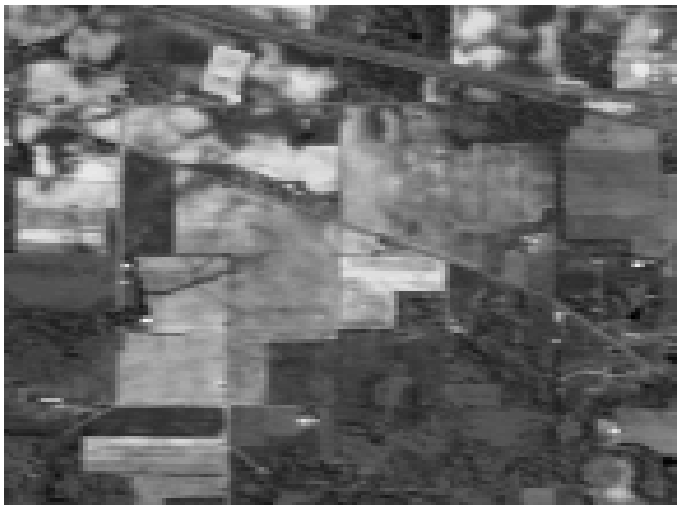

Figure 2: Band 8 (0.58–0.62μm) of AVIRIS Indian pine test site image

to get 6888 opponent features. Thus, a test texture image can be represented by a vector of 7224 unichrome and opponent features. We compute a mean feature vector for each of the 8 texture classes by averaging the feature vectors for all of the test texture images of that texture class.

We define a distance metric between two feature vectors by

$$d_{ij} = \sum_{k=1}^{p} \left(\frac{f_k^i - f_k^j}{\gamma(f_k)} \right)^2 \tag{6}$$

where $(f_1^i, f_2^i, \ldots, f_p^i)$ is the feature vector for texture image i and $(f_1^j, f_2^j, \ldots, f_p^j)$ is the feature vector for texture image j. $\gamma(f_k)$ is the standard deviation of f_k over the 8 texture classes. For each test texture image, we compute the distance of the test texture image from the mean feature vector for each of the eight texture classes using (6). We classify a test texture image as an instance of nearest class. We can use a stepwise optimal algorithm to build up approximately optimal feature subsets. At each step, we add a new feature that leads to a maximum increase in classification rate.

3.4 Classification results

We show a comparison of the classification performance for the best subsets of six feature sets in Fig. 5. The first feature set includes the 42 mean features and 42 variance features. The mean feature is defined by $m_i = \frac{1}{100} \sum_{x,y} L_i(x,y)$ with $L_i(x,y)$ denoting the ith spectral band. The variance feature is defined by $var_i = \frac{1}{100} \sum_{x,y} (L_i(x,y) - m_i)^2$. The second feature set includes only the 42 mean features. The third feature set includes only the 42 variance features. The fourth feature set includes the 336 unichrome features. The fifth feature set includes the 6888 opponent features. The sixth feature set includes all 7224 unichrome and opponent features. We see that for a given number of features, the mean and variance feature set performs better than only the mean or only the variance feature set. The unichrome feature set performs better than the mean and variance feature set. We also see that using the opponent features significantly improves the classification accuracy over only using the unichrome features.

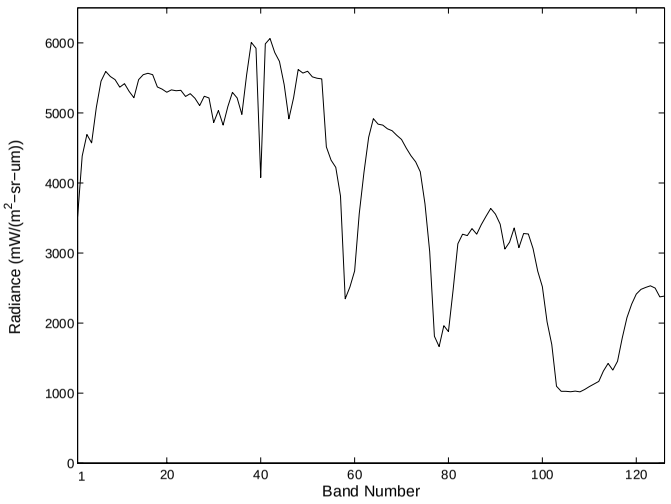

Figure 3: AVIRIS spectral signature (bands 1–126)

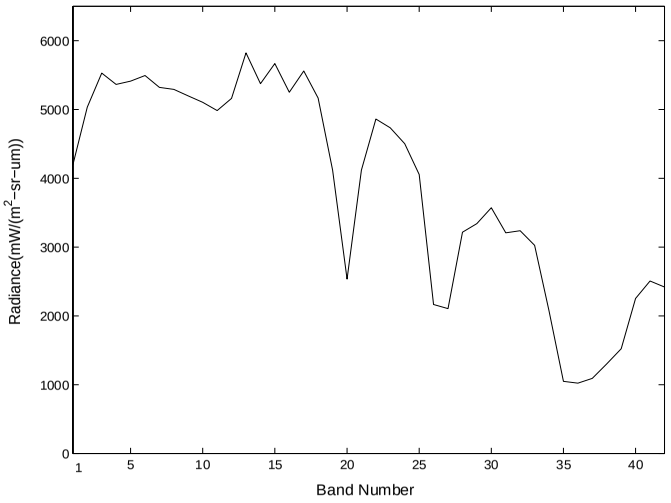

Figure 4: Spectral signature in the reduced band system (bands 1–42)

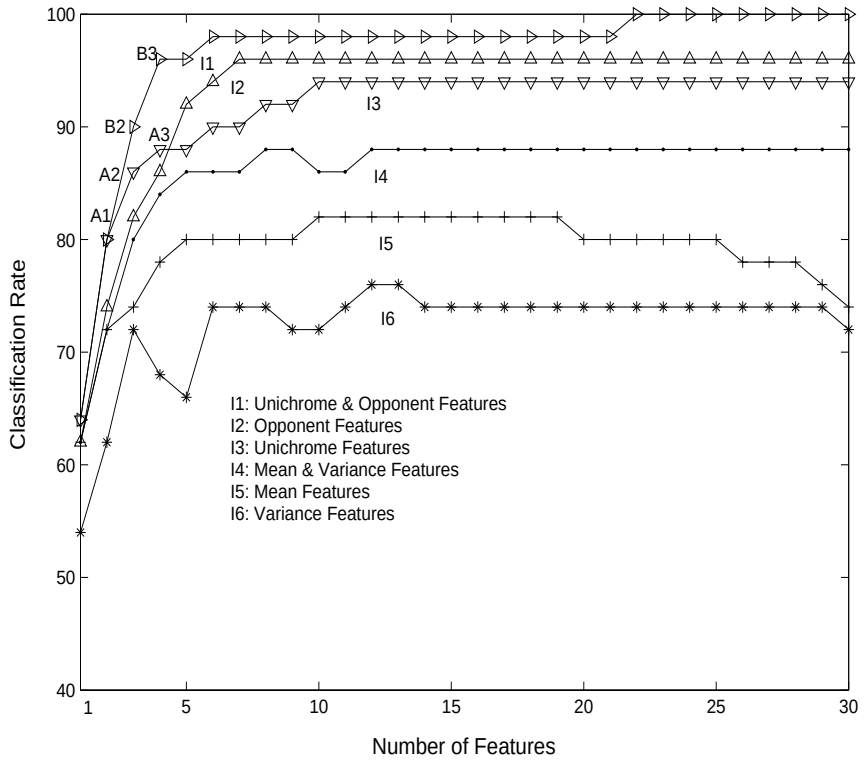

Figure 5: Best classification rate for each of six feature sets

3.5 An example

Texture class 1 (Corn-notill) and texture class 2 (Corn-min) are taken as an example to illustrate how the use of opponent features improves classification performance. There are seven test texture images of size 10×10 in class 1 and five test texture images of size 10×10 in class 2. We define a unichrome filtered image by $|h_{imn}(x, y)|$ and an opponent filtered image by $|d_{ijmn}(x, y)|$ so that the square of the unichrome feature defined by (3) is the energy of the unichrome filtered image and the square of the opponent feature defined by (5) is the energy of the opponent filtered image. We label several points in figure 5 with A_i or B_i symbols. We denote the best two unichrome features at A_1 as μ_1, μ_2, the added unichrome feature at A_2 as μ_3, and the added unichrome feature at A_3 as μ_4. Point B_1 coincides with point A_1 since the best two selected features from the unichrome and opponent feature set are only unichrome features. We then denote the added opponent feature at B_2 as ψ_1 and the added opponent feature at B_3 as ψ_2. Fig. 6 displays the filtered images for the seven 10×10 instances of texture 1. From top to bottom in Fig. 6 are filtered images corresponding to $\mu_1, \mu_2, \mu_3, \psi_1$ and ψ_2. Similarly, the filtered images for the five instances of texture 2 are shown in Fig. 7. We see that while the unichrome filtered images for the two texture classes are quite similar, the opponent filtered images are significantly different. The opponent filtered images for texture class 1 have more energy than the opponent filtered images for texture class 2. This can also be seen by examining the computed features shown in Table 1. The values of μ_1, μ_2, and μ_3 are close for the two classes while the values of ψ_1 and ψ_2 are significantly larger for class 1 than for class 2.

Using (6), we also compute the distance between the mean of the seven instances of texture class 1 and the mean of the five instances of texture class 2 at points A_1, A_2, A_3, B_2 and B_3. The results are shown in Table 2. For a fixed number of features, the distance increases greatly with the opponent features added to the feature

set. This indicates that texture classes 1 and 2 are more easily discriminated when using the opponent features versus only unichrome features.

To show why the opponent features improve classification performance, we consider the first selected opponent feature ψ_1 which captures the spatial correlation between band 9 and band 28 at a certain scale and orientation. ψ_1 is much larger for texture class 1 than for texture class 2 which suggests that the band 9 and band 28 intensities across rows are more correlated for texture class 2 than for texture class 1. If normalized band 9 and band 28 are equal, then from (4) the opponent feature ψ_1 will be zero. We compute normalized intensities of band 9 and band 28 for texture class 1 along a row by averaging the rows of the filtered image for these two bands respectively. The normalized intensities are plotted in Fig. 8. Similarly, we plot the normalized intensities for texture class 2 in Fig. 9. As we can see, the normalized band 9 and band 28 curves are more similar for texture class 2 than for texture class 1.

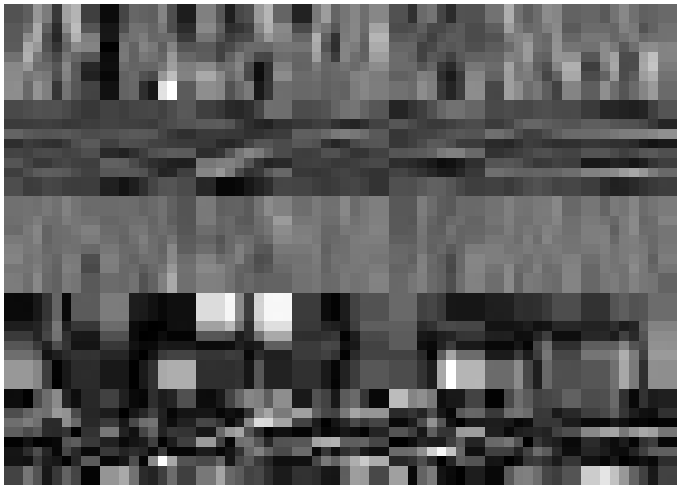

Figure 6: Filtered images for texture 1 (from top to bottom: $\mu_1, \mu_2, \mu_3, \psi_1, \psi_2$)

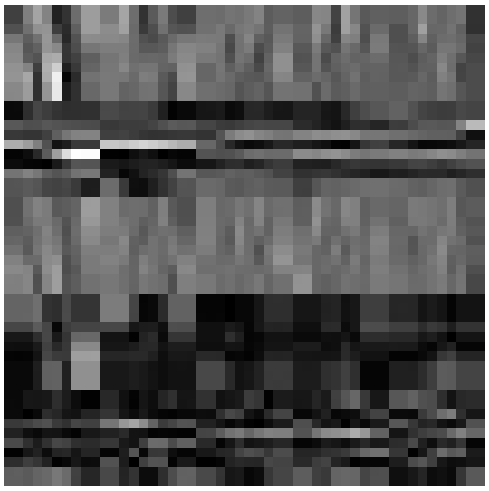

Figure 7: Filtered images for texture 2 (from top to bottom: $\mu_1, \mu_2, \mu_3, \psi_1, \psi_2$)

Table 1: Selected features for texture 1 and 2

	Texture 1	Texture 2
μ_1	0.0320	0.0312
μ_2	0.0228	0.0258
μ_3	0.0133	0.0132
ψ_1	0.0452	0.0256
ψ_2	0.1335	0.0964

Table 2: Distance metrics between texture 1 and 2

	Number of Features	Distance Metrics
A_1	2 uni	1.6203
A_2	3 uni	1.6260
A_3	4 uni	1.6298
B_2	2 uni 1 oppo	1.8742
B_3	2 uni 2 oppo	2.1826

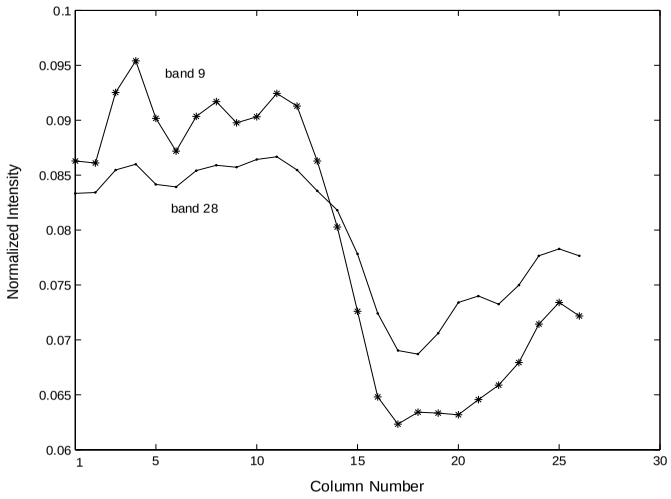

Figure 8: Normalized intensities of band 9 and band 28 across rows for texture 1

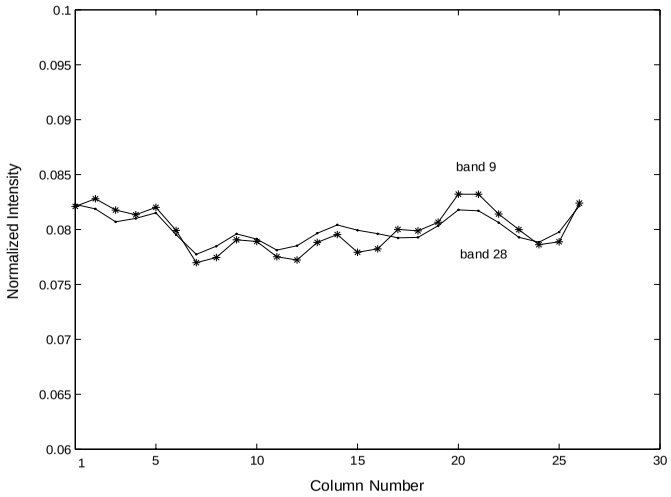

Figure 9: Normalized intensities of band 9 and band 28 across rows for texture 2

4 SUMMARY

In this paper, we have examined feature subspaces for texture recognition in hyperspectral imagery using unichrome and opponent features computed from Gabor filter outputs. The opponent color features are motivated by opponent processes in human vision. With the unichrome and opponent features, we can capture the spatial information within and between spectral bands. Using an AVIRIS data set, we demonstrated the discriminatory power of optimized feature sets that include opponent features for texture recognition. We have shown that using both unichrome and opponent features significantly improves the performance of texture classification over only using the same number of unichrome features.

5 ACKNOWLEDGMENTS

This work has been supported by the National Science Foundation and the Air Force Office of Scientific Research.

References

Basedow, R. W., D. C. Armer, and M. E. Anderson, 1995, "HYDICE system: Implementation and Performance," *SPIE Proceedings*, Vol. 2480, 258–267.

Bovik, A. C., M. Clark, and W. S. Geisler, 1990, "Multichannel texture analysis using localized spatial filters," *IEEE Trans. Pattern Anal. Machine Intell.*, Vol. 12, pp. 55–73.

Cross, G. R. and A. K. Jain, 1983, "Markov random field texture models," *IEEE*, PAMI, 5: 25–39.

Daugman, J. G., 1985, "Uncertainty relation for resolution in space, spatial frequency and orientation optimized by two-dimensional visual cortical filters," *J. Opt. Soc. Amer.*, Vol. 2, pp. 1160–1169.

Goldstein, E. B., 1996, *Sensation & Perception*, 4th ed. Pacific Grove, Calif., Brooks/Cole Publishing Company.

Haralick, R. M., 1979, "Statistical and structural approaches to texture," *Proc. IEEE*, Vol. 67, 786–804.

Healey, G. and A. Jain, 1996, "Retrieving multispectral satellite images using physics-based invariant representations," *IEEE Trans. Pattern Anal. Machine Intell.*, Vol. 18, pp. 842–848.

Healey, G. and L. Wang, 1995, "Illumination-invariant recognition of texture in color images," *J. Opt. Soc. Amer. A*, Vol. 12, pp. 1877–1883.

Hurvich, L. M. and D. Jameson, 1957, "An Opponent-Process Theory of Color Vision," *Physiological Rev.*, Vol. 64, pp. 384–404.

Jain, A. K. and F. Farrokhnia, 1991, "Unsupervised texture segmentation using Gabor filters," *Pattern Recognit.*, Vol. 24, pp. 1167–1186.

Jain, Amit and G. Healey, 1998, "A Multiscale Representation Including Opponent Color Features for Texture Recognition," *IEEE Trans. Image Processing*, Vol. 7, No. 1.

Kondepudy, R. and G. Healey, 1994, "Use of invariants for recognition of three-dimensional color textures," *J. Opt. Soc. Amer.*, Vol. 11, pp. 3037–3049.

Li, S. Z., 1995, *Markov Random Field Modeling in Computer Vision*, Springer.

Mallat, S., 1989, "Multi-resolution approximation and wavelet orthonormal bases of $L^2(R)$," *Trans. Amer. Math. Soc.*, 315: 69–87.

Manjunath, B. S. and W. Y. Ma, 1996, "Texture features for browsing and retrieval of image data," *IEEE Trans. Pattern Anal. Machine Intell.*, Vol. 18, pp. 837–842.

Masland, R. H., 1996, "Unscrambling Color Vision," *Science*, Vol. 271, No. 2, pp. 616–617.

Reed, T. R. and J. M. Hans du Buf, 1993, "A review of recent texture segmentation and feature extraction techniques," *Computer Vision Graphics and Image Processing*, Vol. 3, No. 57, 359–372.

Schweizer, S. and J. Moura, 2001, "Efficient Detection in Hyperspectral Imagery," *IEEE Trans. Image Processing*, Vol. 10, No. 4, 584–597.

Simi, C. G., S. G. Beaven, E. M. Winter, C. LaSota, J. Parish, and R. Dixon, 2000, "Night vision imaging spectrometer (NVIS) performance parameters and their impact on various detection algorithms," *SPIE Proceedings, Algorithms for Multispectral, Hyperspectral, and Ultraspectral Imagery VI*, Vol. 4049.

Vane, G., R. Green, T. Chrien, H. Enmark, E. Hansen and W. Porter, 1993, "The airborne visible infrared imaging spectrometer,"*Remote Sensing of Environment*, Vol. 44, 127–143.

Wiesel, T. N. and D. H. Hubel, 1966, "Spatial and Chromatic Interactions in the Lateral Geniculate Body of the Rhesus Monkey," *J. Neurophysiology*, Vol. 29, pp. 1,115–1,156.